Environmental Pollution 253 (2019) 207–220

Contents lists available at ScienceDirect

Environmental Pollution

journal homepage: www.elsevier.com/locate/envpol

Vertical distribution of the Asian tropopause aerosols detected by CALIPSO☆

Hewen Niu [a, b], Shichang Kang [a, c, e, *], Wanni Gao [d], Yuhang Wang [b], Rukumesh Paudyal [a]

[a] State Key Laboratory of Cryospheric Science, Northwest Institute of Eco-Environment and Resources, Chinese Academy of Sciences, Lanzhou, 730000, China
[b] School of Earth and Atmospheric Sciences, Georgia Institute of Technology, Atlanta, GA, USA
[c] CAS Center for Excellence in Tibetan Plateau Earth Sciences, Beijing, 100101, China
[d] School of International Cultural Exchange, Lanzhou University, Lanzhou, 730000, China
[e] University of Chinese Academy of Sciences (UCAS), Beijing, 10049, China

ARTICLE INFO

Article history:
Received 4 April 2019
Received in revised form
3 June 2019
Accepted 27 June 2019
Available online 10 July 2019

Keywords:
Aerosol
Asian summer monsoon
Tropopause
Vertical

ABSTRACT

Characterizing the vertical distribution of aerosol optical properties is crucial to reduce the uncertainty in quantifying the radiative forcing and climate effects of aerosols. The analysis of four-year (2007–2010) Cloud-Aerosol Lidar and Infrared Pathfinder Satellite Observation (CALIPSO) lidar measurements revealed the existence of tropospheric aerosol layers associated with the Asian summer monsoon. The measurements of five typical aerosol optical and microphysical parameters were used to explore the properties, spatial/vertical distributions, annual evolution of tropopause aerosols over the South Asia region. Results extracted from various latitude-height and longitude-height cross sections of aerosol extinction coefficient at 532 and 1064 nm, backscatter coefficient at 532 nm, and depolarization ratio at 532 nm demonstrated that a large amount of aerosols vertically extended up to the tropopause (12 km) during the monsoon season over the north Arabian Sea, India, north Bay of Bengal, and equatorial Indian Ocean, finally reaching the southeast of the Tibetan Plateau. Convective transport associated with Asian summer monsoon is an important factor controlling the vertical distribution of tropopause aerosols. The evolution of aerosol scattering ratio at 532 nm indicated that from equatorial Indian Ocean to South Asia, there exists an upward tilting and ascending structure of the aerosols layer during the monsoon season, which typically indicates enhanced aerosols over the Asian monsoon region. Information on aerosol size distribution and detailed composition are needed for better understanding the nature and origin of this aerosol layer. Enhancement of the tropopause aerosols should be considered in the future studies in evaluating the regional or global climate systems. Further satellite observations of aerosols and in-situ observations are also urgently needed to diagnose this aerosol layer, which likely originate from anthropogenic emissions.

1. Introduction

The tropical tropopause layer is generally recognized to control the entry of air from troposphere into the stratosphere (Vernier et al., 2011, 2015; Kremser et al., 2016). However, the Asian monsoon circulation offers an alternative way that bypasses the tropical region (Gettelman et al., 2004; Randel et al., 2010). Previous study indicated that convection is strongest in the tropics and aerosols were uplifted to higher altitudes as compared to elsewhere (Holton et al., 1995; Fu et al., 2006). The transport of atmospheric sulfur, mostly produced from the tropic region (Kremser et al., 2016; Vernier et al., 2011, 2015), to higher altitudes by the monsoon wind/air, could affect the chemical balance of atmosphere and the climate (Thomason et al., 2007; Randel et al., 2010; Solomon et al., 2011). Global satellite aerosol data implies a negative radiative forcing (- 0.1 W m^2) due to stratospheric aerosol changes (Solomon et al., 2011; Vernier et al., 2015). Model simulations had suggested that deep convection could efficiently lift human-derived species (e.g., SO_x, NO_x, H_2S) from strong source regions over Asia (Lawrence et al., 2003; Niemeier and Timmreck,

☆ This Paper has been recommended for acceptance by Xiaoping Wang.

* Corresponding author. Present address: Donggang West Road 320, Chengguan district, Lanzhou city, 730000, China.
E-mail address: shichang.kang@lzb.ac.cn (S. Kang).

https://doi.org/10.1016/j.envpol.2019.06.111
0269-7491/

2015; Guo et al., 2017), the atmospheric species could be entrapped and transported to the Eastern Mediterranean Sea along the southern edge of the anticyclone circulation during Asian Summer Monsoon (ASM) (Li et al., 2005; Park et al., 2007; Randel et al., 2010; Lawrence and Lelieveld, 2010; Vernier et al., 2015; Cohen et al., 2018). It has been observed that during the fast convective, tropospheric air can directly enter into the lower stratosphere over the Tibetan Plateau (TP) (Fu et al., 2006). In addition, numerical simulations suggest that 75% of the total summer water vapors were transported into the global tropical stratosphere, which may easily occur over the South Asian monsoon regions (Gettelman et al., 2004; Li et al., 2005; Kim et al., 2003).

Given the underlying impacts of aerosol on the radiative forcing of the tropopause, a key scientific question is whether natural and/or anthropogenic aerosols and their gas-precursors can also be transported to the upper troposphere by deep convection during the ASM. However, there are substantial obstacles to this transport because, generally, aerosols are effectively scavenged by frequent rainfall events in ASM season (Rosenfeld et al., 2007; Mari et al., 2010; Niu et al., 2014, 2018). Moreover, heterogeneous aerosol processing may change the hygroscopicity (Cohen et al., 2018; Wang et al., 2006), which in turn affects the scavenging efficiency and vertical distribution of the aerosols (Kim et al., 2008; Cohen and Prinn, 2011). These components have been revealed to interact and combine each other, the slight changes in their premier vertical distribution can result in distinct discrepancies in atmospheric transport thousands of kilometers apart (Tao et al., 2012; Wang, 2013; Pei et al., 2019). Therefore, characterizing the vertical distribution of aerosols properly is important to restrict their atmospheric spatial-distribution and climatic effects, which also impact the atmospheric energy balance (Cohen et al., 2018; Kim et al., 2008), atmospheric circulation, and precipitation (Ming et al., 2010; Tao et al., 2012; Wang, 2013; Li et al., 2015). Large scale variability of atmospheric deep convection accounts for most of the vertical transport of energy from the planetary boundary layer (PBL) to upper troposphere and rainfall (Rajeevan et al., 2013).

However, aerosol field observations in the upper troposphere either from satellites or other instruments have been very scarce. Recent investigations of aerosol layer in the upper troposphere from the Cloud-Aerosol Lidar with Orthogonal Polarization (CALIOP) lidar (Thomason et al., 2007; Winker et al., 2007, 2010; 2013; Yu et al., 2010; Tian et al., 2017) have identified a notable amount of non-volcanic aerosol near the tropopause during the ASM (Anderson et al., 2003; Fu et al., 2007; Thomason and Vernier, 2013), which was named the Asian Tropopause Aerosol Layer (ATAL) (Vernier et al., 2011, 2015). Tropospheric aerosols are largely variable in terms of time and space (e.g., Winker et al., 2007; Vernier et al., 2011), satellite observations are urgently needed to well understand the distribution and impact of aerosols on regional and global scales. This study deeply surveys the optical characteristics, vertical distributions, formation mechanisms, and possible sources of the ATAL.

The CALIOP lidar, onboard the Cloud-Aerosol Lidar and Infrared Pathfinder Satellite Observation (CALIPSO) satellite, has been acquiring global aerosol profile and layer data since June 2006 (Winker et al., 2007, 2010), the observations crossing the latitudes from 82° S to 82° N. CALIPSO is in an earth sun-synchronous pathway at a 705 km height, and with a 16-day orbit repeat-cycle (Liu et al., 2008a; Winker et al., 2013; Vernier et al., 2015). One limitation of the CALIPSO is that its global sampling coverage takes 16 days. CALIOP aerosol profile products (e.g., Level 2 and 3) have been extended to provide a three-dimensional view of the global distribution of atmospheric aerosols. CALIOP is a nadir-viewing instrument and only acquires measurements along the satellite ground-track (Cohen et al., 2018; Winker et al., 2013). The global investigation of vertical profiles of aerosols from CALIPSO observations provides many options to study vertical distribution of aerosol and to improve parameterization of aerosol in the climate and weather-forecast models (Liu et al., 2017; Thomason et al., 2007; Rajeevan et al., 2013). In this paper, four-year (2007–2010) satellite observations of tropospheric aerosols from the CALIPSO have been performed to examine the vertical distribution of aerosols associated with the ASM, and particularly the mean vertical distribution and its variability during the active and break monsoon spells/periods. Section 2 provides a description of CALIPSO satellite measurements used in this study and the statistic methods employed in data processing. In section 3, we focused on the vertical distribution of tropospheric aerosols during the active and break spells investigated by using microphysical and optical parameters of aerosol. We have examined annual vertical structure of tropopause aerosols using aerosol scattering ratio at 532 nm. Finally, mechanisms responsible for the formation of ATAL and its origin are discussed and concluded.

2. Data and methodology

2.1. Description of CALIPSO

The primary objective of CALIPSO is to provide measurements that can improve our understanding of the role of aerosol in the climate system (e.g., Winker et al., 2007, 2010). The primary task of CALIPSO is devoted to the detection of aerosols vertically from the whole troposphere to the lower stratosphere (Vernier et al., 2011; Winker et al., 2010). The CALIPSO payload consists of three instruments, including the Cloud-Aerosol Lidar with Orthogonal Polarization (CALIOP) and two others (Winker et al., 2007; Thomason et al., 2007). CALIPSO detects the aerosol at global-scale with an absolutely high resolution and sensitivity, its vertical resolution is 60 m in the upper troposphere (<20.3 km) (Thomason et al., 2007; Winker et al., 2010). The highest detecting resolution is 1/3 km horizontally and 30 m vertically (height: −0.5 km - 8.2 km) for the 532 nm data. The vertical resolution of the aerosol profile data changes with altitude. The highest resolutions are employed for the lower altitudes where aerosol generally has a larger spatial variability and stronger backscatter intensity (Liu et al., 2008b). Data from these equipments are used to explore the vertical distributions of aerosols in the atmosphere, as well as aerosols optical and microphysical properties which influence the Earth's radiation budget. CALIOP provides profiles of total attenuated backscatter coefficients at wavelengths of 532 and 1064 nm, and two perpendicular and parallel polarization components. The estimates of aerosol particle size can be obtained from the depolarization ratios at the two wavelengths. Aerosol heights and the extinction coefficient (at 532 or 1064 nm) data can be extracted/retrieved from the total backscatter coefficients.

In this study, five parameters which closely associated with aerosol optical and microphysical properties are employed: aerosol extinction coefficient at 532 and 1064 nm, total backscatter coefficient at 532 nm, particulate depolarization ratio profile at 532 nm, as well as aerosol scattering ratio at 532 nm. Profile data for tropospheric aerosols is retrieved from the CALIPSO.

2.2. CALIPSO measurements of aerosols in the troposphere

The CALIOP data set has been arranged in a series of 16-day time resolution 3-D grids of 1° latitude × 1° longitude × 1 km height. The Scattering Ratio (SR) is calculated using the total backscatter (aerosol + molecular) coefficients and the molecular alone (Vernier et al., 2009).

For the 532 nm data, the particulate total backscatter

coefficients are derived from the sum of the parallel and perpendicular backscatter measurements recorded aboard the CALIPSO satellite (i.e. $\beta_{532\ total} = \beta_{532\ parallel} + \beta_{532\ perp}$).

The vertical structure of aerosols has been examined by analyzing the vertical distribution of extinction coefficient and total backscatter coefficient, as well as particulate depolarization ratio. For examining vertical structure, we have evaluated several vertical cross sections over the ASM region, e.g., latitude-height cross section and longitude-height cross section. The latitude-height section is identified to examine the north–south variation of aerosol properties along the north Arabian Sea and the Bay of Bengal and the south of TP.

Extensive global observations have revealed the break and active monsoon phases during the ASM over the Indian subcontinent. The two phases have an overlap of 30–60 days and 10–20 fluctuations (Rajeevan et al., 2010, 2013). During the break (active) spells, suppression (intensification) of deep convection activity occurs over the Indian subcontinent (Ravi Kiran et al., 2009). During the break phase, the monsoon trough is located near the foothills of the Himalayas which cause distinct decrease of rainfall. In this study, employing the break and active phases during the monsoon period, as identified by Rajeevan et al. (2010, 2013) and Ravi Kiran et al. (2009), we thoroughly determined the vertical distribution of aerosols associated with active and break phases over the ASM region. Using the CALIPSO data for the monsoon seasons in 2007, 2008, 2009, 2010, the vertical profiles (longitude and latitude-height cross sections) of the five optical and microphysical parameters of aerosols over the ASM regions were identified.

3. Results and discussion

3.1. Optical properties of Asian tropopause aerosol

A typical profile of the CALIPSO observation over the summer monsoon region has been retrieved and displayed in Fig. 1, which represents aerosol extinction coefficient at 532 nm on 13 August 2007 as a function of heights. It generally demonstrates the vertical distribution of tropopause aerosol-signal over the study area of this work. The spatial distribution of the mean aerosol extinction coefficient at 532 nm over the ASM region during July and August in 2007, 2008, 2009, and 2010 has been shown in Fig. S1. Tropospheric aerosols were more and more extensive from southwest to northwest of the region. In addition, among the investigated years, the average aerosol extinction coefficient in 2009 was higher, which probably indicates stronger aerosols or airborne dust emissions from Pakistan, Afghanistan, north Arabian Sea, and west of India during the summer monsoon season (Liu et al., 2008a). The vertical profiles of aerosol extinction coefficient, total backscatter coefficient and particulate depolarization ratio derived from CALIPSO at 532 nm during the ASM of 2007–2010 are shown in Fig. 2. Maximum aerosol extinction coefficient is observed over the west coast of India and the southwest of the TP. The most obvious aerosols are vertically homogeneously distributed below the PBL height, but they vertically extended beyond 10 km in the troposphere (Fig. 2 a, d). The vertical distribution of aerosol extinction coefficient observed from the latitude-height cross section indicated that aerosols were transported from south to north over the ASM region. In addition, over the west coast of India and the north Arabian Sea, the most pronounced extinction coefficient of aerosol has been observed over the North Bay of Bengal (Fig. 2a, d). The vertical distribution of total backscatter coefficient of aerosol has the similar trend with that of aerosol extinction coefficient (Fig. 2b, e). However, aerosol total backscatter coefficients are marginally smaller than extinction coefficients over the ASM region. It was identified that a lower planetary boundary layer height also contributes to higher aerosol loading near the ground surface (Guo et al., 2016). Strong vertical mixing in summer transports more aerosols from the atmospheric boundary layer to the free

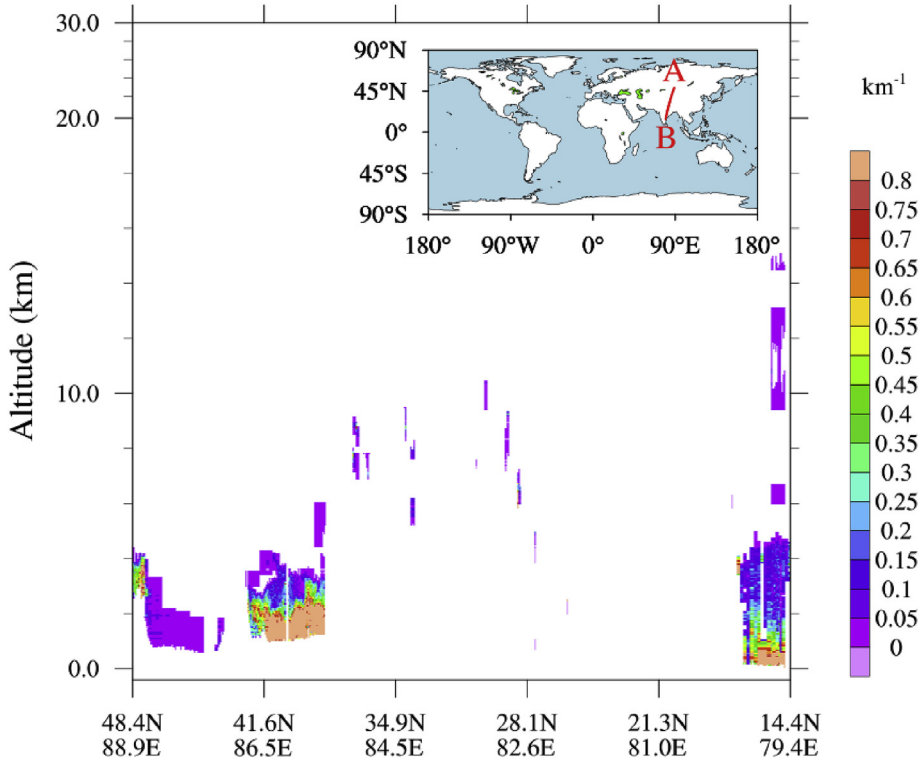

Fig. 1. Profile of the aerosol extinction coefficient at 532 nm (unit: km^{-1}) over the Asia summer monsoon region on August 13, 2007 detected by CALIPSO.

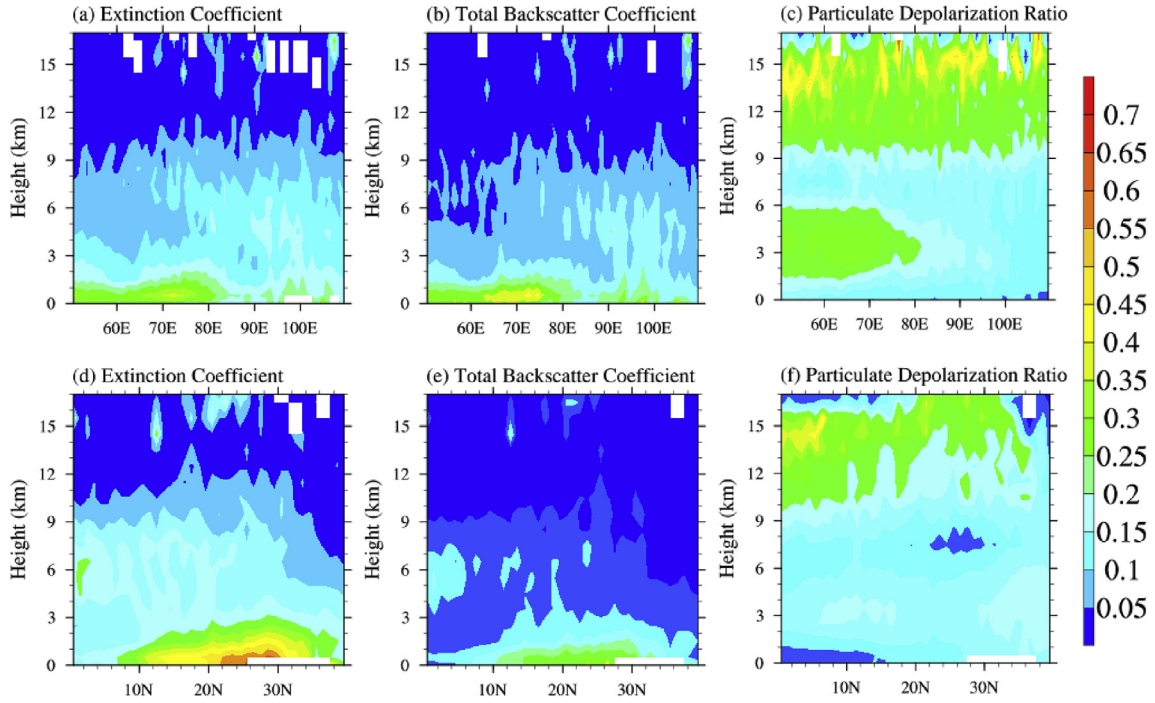

Fig. 2. Longitude-height cross section (upper panel) and latitude-height cross section (lower panel) of the mean aerosol extinction coefficient (unit: km^{-1}), total backscatter coefficient (unit: km^{-1} sr^{-1}), and particulate depolarization ratio at 532 nm from CALIPSO during the monsoon periods of 2007–2010. The latitude and longitude bounds are from 0° N to 40° N and from 50° E to 110° E, respectively.

troposphere (Tian et al., 2017). Based on the longitude-height cross sections of aerosol extinction coefficient and total backscatter coefficient (Fig. 2a and b), we can observe that there is a vertical tilting structure of enhanced aerosol optical properties over the north Bay of Bengal and southeast of TP. The enhanced aerosol extinction coefficient and backscatter coefficient probably associated with boreal summer intra-seasonal variability (BSISV) (Jiang et al., 2011). Moreover, it was observed that aerosols within PBL height have distinct seasonal variation (Tian et al., 2017). The vertical structure of tropopause aerosol could be an indicative of a pre-conditioning process for the northward propagation of BSISV (Rajeevan et al., 2013; Jiang et al., 2011). Lidar and balloon-borne measurements demonstrated that appearance of cold tropopause and increase in moisture in the upper troposphere (Park et al., 2007) are considered to be important factors to explain the enhancement of tropopause aerosol observed in summer over the TP (Kim et al., 2003).

Different with the vertical distribution of aerosol extinction coefficient and total backscatter coefficient, three-dimensional structure of particulate depolarization ratio has more distinct characteristics over the ASM region. From the longitude-height cross section we noticed that the depolarization ratio is higher over the north Arabian Sea, the west coast of India, as well as the southwest of TP, which corresponded to an elevated aerosol or dust layer transported from west to east at heights of 1–6 km over these regions. Depolarization ratio was normally used as an indicator to separate dust from other types of aerosols (Murayama et al., 2001; Huang et al., 2008; Haarig et al., 2018). High depolarization ratio in the west of the region (Fig. 2c) probably indicates dust was lofted and advected over the north Arabian Sea and the west coast of India. It is well known that dust events occur frequently as sources over the Arabian Peninsula through western India (Wang, 2009; 2018; Liu et al., 2008a). Located in the dust belt, the Arabian Peninsula is a major source of atmospheric dust. Frequent dust outbreaks (15–20 dust storms per year) have profound impacts on all aspects of human activities and natural processes in this region (Prakash et al., 2015; Jin et al., 2016). Moreover, another enhanced aerosol layer over the entire ASM region considerably extended even up to 16 km in the tropopause which can be identified by the maximum particulate depolarization ratio (Fig. 2c). The vertical distribution of the enhance aerosol layer over the ASM region can further be verified in latitude-height cross section (Fig. 2f). It is worth noting that the elevated aerosol layer was extensively transported from the equatorial Indian Ocean, crossed over the North Bay of Bengal and finally reached the southeast of the TP. High depolarization ratio in the eastern part of the region (Fig. 2c) suggests that the tropopause aerosols were probably composed of urban aerosols and biomass burning aerosols, which have different depolarization ratios. Therefore, those aerosols were carried upward by convection and trapped into the tropopause region. Previous study recognized that over the North Bay of Bengal, deep convective clouds with the maximum altitude above 16 km were also detected (Rajeevan et al., 2013), which greatly consistent with the vertical distribution of tropopause aerosol found in this study. Convective transport has been identified as an important factor that controls the vertical structure of tropopause aerosols (Kipling et al., 2016). A recent re-analysis of Stratospheric Aerosol and Gas Experiment II satellite observations has confirmed the enhancement of aerosol associated with the ASM from the early 2000s (Thomason and Vernier, 2013; Vernier et al., 2015). ATAL during the ASM has extended vertically up to the tropopause and was confined by the Asian anticyclone (Vernier et al., 2011) which enables the transport of air masses from Southeast Asia (Lawrence and Lelieveld, 2010). The ATAL probably is of non-volcanic aerosols for the global upper troposphere.

3.2. Vertical structure of tropopause aerosol during the active and break spells

It is generally recognized that during the boreal-summer monsoon season, substantial climate variability (on daily, seasonal, inter-annual, and decadal time scales) of convection and rainfall over the ASM region arises from the oscillation on the intra-seasonal scale between active and break spells. It is important to understand the physical mechanism of the active and break spells and transition from the active to break phases. Light-absorbing (e.g., carbonaceous aerosols) aerosols in tropopause layer play an important role, especially in the transition of Indian monsoon from break to active spells. Manoj et al. (2011) proposed that absorbing aerosols modulate the north-south temperature gradient at lower levels during the transition period, and facilitate the transition of Indian monsoon from breaks to active phases. Both the dynamical and thermo-dynamical factors might play an important role in modulating the intra-seasonal activity of ASM and thus causing the active and break spells during the ASM. Moreover, absorbing aerosols have a strong influence on the monsoon circulation and the development of convective precipitation, aerosol induced perturbations can affect Indian summer monsoon circulation and precipitation (Wang, 2009). The distinct meridional evolution of intraseasonal variability from the equatorial zone to the Indian continent modulates of the active/break phases of the south Asian monsoon (Jiang et al., 2011). A number of studies using different general circulation models indicate that direct radiative forcing of carbonaceous aerosols can result in northward shift of precipitation in the intertropical convergence zone (Wang, 2009). Recent modeling studies also suggest that direct radiative forcing of aerosols has a significant influence on Indian summer monsoon (Lau et al., 2008, 2016). Radiative forcing of carbonaceous aerosols can enhance the Indian summer monsoon circulation (Wang, 2004; 2007). Ramanathan et al. (2005) found that an increase in the black carbon radiative forcing over the Indian subcontinent and surrounding areas leads to changes in monsoon and pre-monsoon tropical convective precipitations. In the northern precipitation-band of the Intertropical Convergence Zone, its precipitation has an enhancement of 15% due to the direct forcing of black carbon aerosols (Wang, 2007).

The mean vertical profiles of aerosol extinction coefficient over the ASM region associated with active and break spells are retrieved and are shown in Fig. S2 (a - d). Maximum of aerosol extinction coefficient is observed over the northwest Arabian Sea and the west coast of India, where it is extended vertically up to more than 5 km (Fig. S2a) during the active spell, and it is extended vertically 4 km during the break spell (Fig. S2b). In addition, maximum aerosol extinction coefficient is observed over the northwest coast of India and north Arabian Sea, where it is extended vertically up to 5 and 4 km during the active and break spells, respectively (Figs. S2c and d). It is obvious that during the active spell, the aerosol extinction coefficient is extended vertically to altitude higher than that during the break spell, and thus a vertical tilting structure of enhanced aerosol optical properties associated with the ASM over the northwest coast of India and north Arabian Sea can be clearly identified. It is widely recognized that the ASM is one of the most dominant tropical circulation systems in the general circulation of the atmosphere, atmospheric aerosols affect the circulations of the atmosphere by modulating the spatial distribution of heating within the atmosphere and at the surface. In addition, during the active spells, large scale convection can be observed over the western parts of India and the adjoining north Arabian Sea and North Bay of Bengal; suppressed convection was mainly observed during the break spells over the northeast India (e.g., Rajeevan et al., 2013), this is consistent with the spatial trend of the enhanced aerosol extinction coefficient over these regions. The enhanced aerosol layer demonstrated by extinction coefficient measurements during active and break phases in the troposphere probably consisted of dust and anthropogenic aerosols from biomass burning and urban emissions. Generally, extinction coefficients at the two wavelengths (532 and 1064 nm) are quite different, particularly for the larger dust particles and the smaller urban and biomass burning particles. It was proposed that mixtures of anthropogenic aerosols and dust were commonly detected by CALIOP over the southern slope of the TP and a large area in South Asia (Liu et al., 2008a). The latitude-height cross sections (0° N - 40° N) of extinction coefficient at 1064 nm averaged between 50° E – 65° E and 65° E – 80° E associated with active and break phases during the ASM period are shown in Fig. S3. The vertical distributions of aerosol extinction coefficient at 1064 nm (Fig. S3) and 532 nm (Fig. S2) are a little different. The tilting structure generated from 1064 nm extinction coefficient is more distinct compared to from 532 nm, particularly during the active monsoon phase. The enhanced aerosols might be composed of anthropogenic aerosols and airborne dust in the troposphere over the ASM region. Tropospheric aerosols and airborne dust have different sources over the ASM region. Generally, urban and biomass burning emissions are major anthropogenic aerosol sources in the ASM region. Biomass burning represents a major source of pollution throughout the troposphere, with strong impacts on the atmospheric composition (e.g., Hodzic et al., 2007; Konovalov et al., 2011; Yamasoe et al., 2015; Petetin et al., 2018). Urban aerosol is also a major component of tropospheric aerosol, most of the particles in urban aerosol are by-products of photochemical reactions involving nitrogen and hydrocarbons oxides, which are emitted from combustion (Hill and Smoot, 2000).

In order to understand the variability of three dimensional aerosol vertical structure during the active and break monsoon spells, we investigated the total backscatter coefficient of aerosol using the latitude-height cross sections (0°–40° N). The latitude-height cross sections were averaged between 50° and 65° E and 65°–80° E both during the active and break spells associated with the ASM (Fig. 3). It is notable that during the active spells, the spatial distribution of the total backscatter coefficient was vertically extended up to 6 km over north Arabian Sea and the northwest of India (Fig. 3a, c). During the break spells, atmospheric aerosols were vertically extended up to 4 km over those regions. However, most pronounced aerosol occurred in the lower troposphere (below 2 km) either during the active spells or during the break spells (Fig. 3). This is due to extensive convection has lifted the human-derived species (e.g., SO_2, NO_x, dust) from source regions in South Asia (e.g., Cong et al., 2015; Niemeier and Timmreck, 2015; Howarth, 1998; Mitchell, 1970; Zhang et al., 2017). The atmospheric aerosols could almost be transported over the TP during the ASM demonstrated in Fig. 3 (c, d). During the active spells, enhanced aerosol extinction coefficient and total backscatter coefficient suggesting deep convection of atmospheric aerosol over the west coast of India and the north Arabian Sea (Fig. S1c, Fig. 3c). This phenomenon is consistent with the results of vertical cloud structure of the Indian summer monsoon investigated by Rajeevan et al. (2013). The spatial distribution of tropopause aerosol associated with the break and active monsoon spells we found are part of large scale perturbations over the ASM region which comprising other regional heat sources of the ASM.

In addition to the intra-seasonal variability of total backscatter coefficient of aerosol, we investigated the vertical aerosol structures with the microphysical parameter of particular depolarization ratio averaged between 50° and 65° E and 65°–80° E associated with active and break spells during the ASM period. Maximum particular depolarization ratio is observed over the equatorial

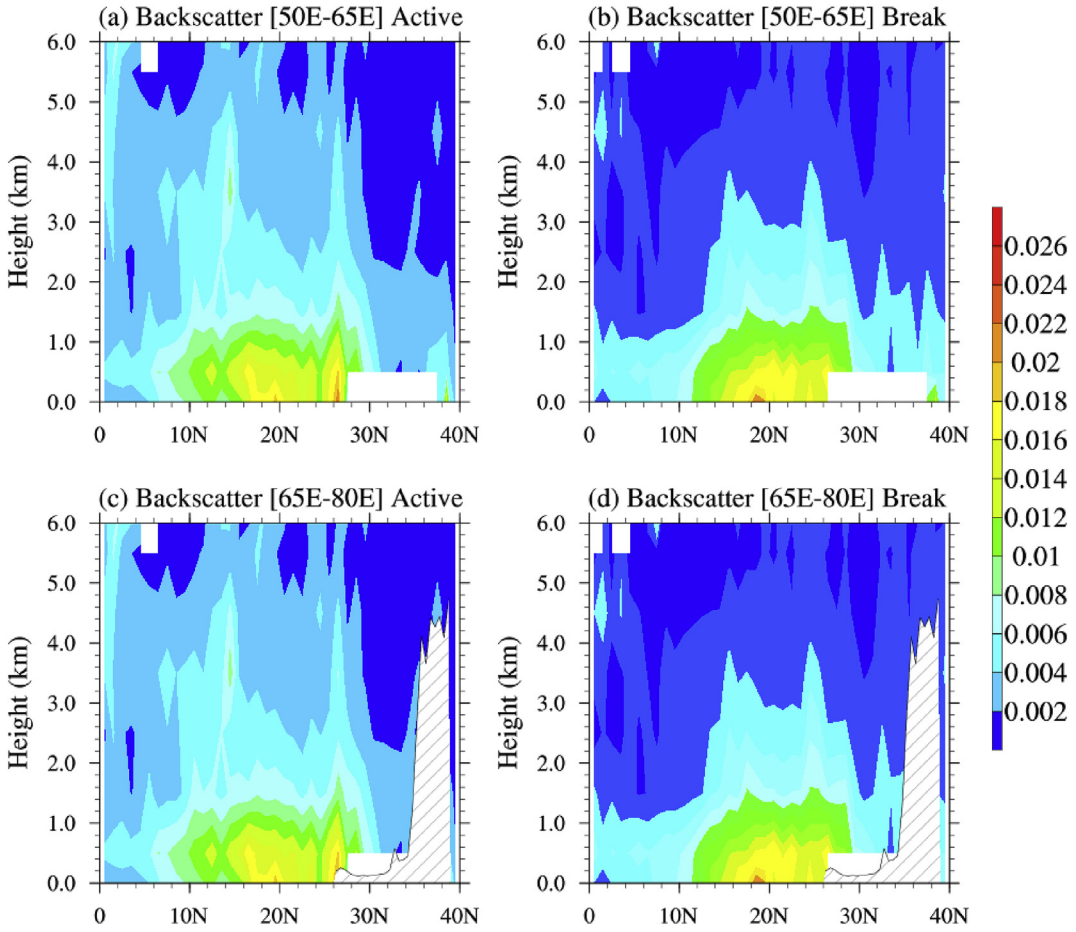

Fig. 3. Latitude-height cross sections (0°–40° N) of aerosol total backscatter coefficient at 532 nm (unit: km^{-1}) averaged between 50° and 65° E and 65°–80° E associated with active and break spells during the ASM period. The shaded parts in plots (c) and (d) indicate the topography of the Tibetan Plateau.

Indian Ocean, north Arabian Sea, the west of India, and the southwest of the TP during the active spell associated with the ASM (Fig. 4a, c), it vertically extends to 6 km over these regions due to large scale convection. The distinct vertical tilting structure of enhanced particular depolarization ratio during the active spell anomalies may be relevant to the BSISV (Jiang et al., 2011), moreover, the vertical tilting structure of aerosol suggests a preconditioning process for the northward spread/diffusion of the BSISV, it is well recognized that a wide range of convection was observed over the west of India and the surrounding north Arabian Sea (Rajeevan et al., 2013). During the break spell, the vertical distribution of aerosol particulate depolarization ratio from the latitude-height cross-sections nearly has not presented remarkable trend (Fig. 4b, d), which can be attributed to suppressed convection over the western India during the break period (e.g., Ravi Kiran et al., 2009; Rajeevan et al., 2013).

It is interesting that the enhanced aerosol depolarization ratio can be found over the eastern region of India and adjoining Northern Bay of Bengal, and other adjoining countries in South Asia, i.e. Burma, Laos, and Thailand (Fig. 5). The vertical tilting structure of enhanced particular depolarization ratio extends up to 6 km either during the active (Fig. 5a, c) or break monsoon spells (Fig. 5b, d) over the east of South Asia, as well as the southeast of TP, which suggesting an equatorial and eastward shift of monsoon convection. Previous study suggested that the presence of dust at an altitude of 5 km was detected using the depolarization ratio. The depolarization ratio of dust is high due to the nonsphericity of the dust particles (Murayama et al., 2001), whereas this ratio is low (close to zero) for other aerosol types (Lau et al., 2018). The vertical tilting structure of the enhanced depolarization ratio probably indicates dust aerosol over this region due to strong monsoon convection. Moreover, pollution aerosols and mixtures of pollution aerosols and airborne dust were commonly observed by CALIOP over the southern slope of the TP and a large area to the south (Lau et al., 2018). During the active spell, the vertical structure of aerosol is more extensive compared with the break phase (Fig. 5a, c), indicating large scale convection was significantly prevailing over this region. The ASM system is characterized by deep convective transport of boundary layer air into the upper troposphere over South East Asia which is horizontally and vertically advected by an anticyclone (Liu et al., 2008a, b; Vernier et al., 2011). The enhanced aerosol depolarization ratio firmly demonstrates a vertical structure of aerosol associated with ASM over the east of South Asia. Overall, it is worth noting that an elevated aerosol layer at heights from 1 to 5 km is identified in the west (50°–65° E) and east (80°–105° E) regions of the South Asia.

3.3. Annual variation of tropopause aerosol

In addition to the general characteristics of tropospheric aerosol associated with ASM, we further investigated the spatial and temporal distribution of tropospheric aerosols using the annual dataset of aerosol extinction coefficient. Fig. 6 shows the latitude-height cross section (Fig. 6a, b, c, d) and longitude-height cross

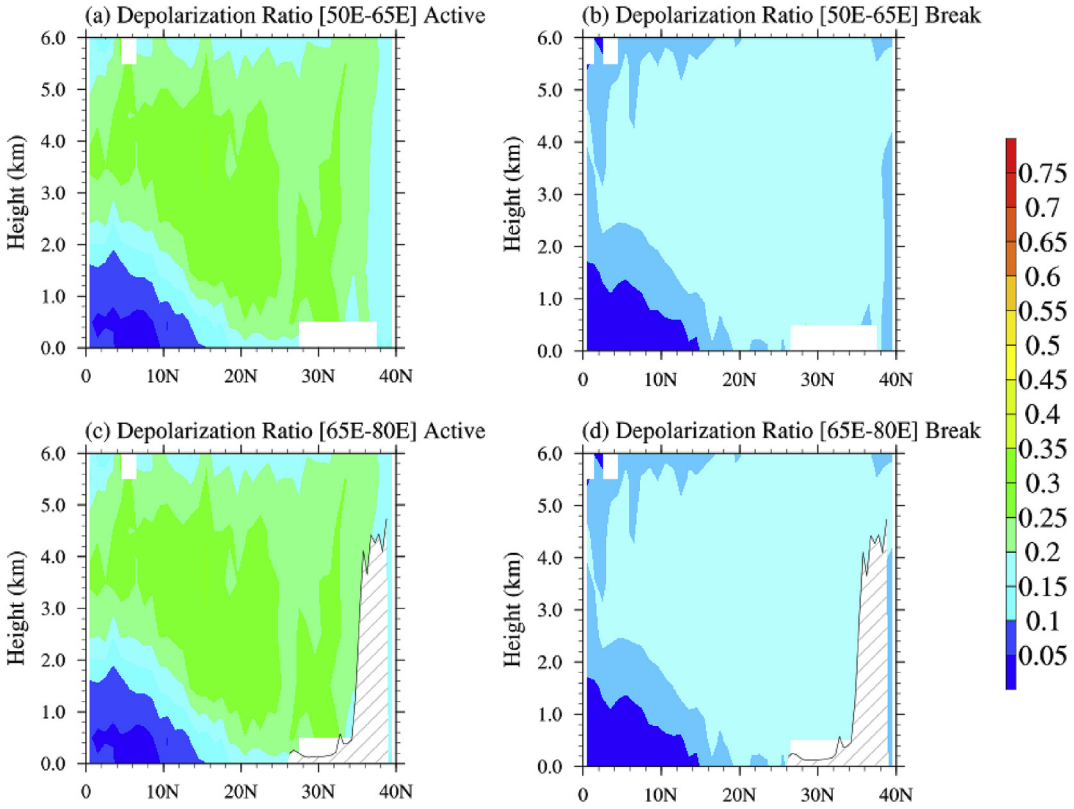

Fig. 4. Latitude-height cross section of particulate depolarization ratio at 532 nm averaged between 50° and 65° E and 65°–80° E associated with active and break spells during the ASM period. The shaded parts in plots (c) and (d) indicate the topography of the Tibetan Plateau.

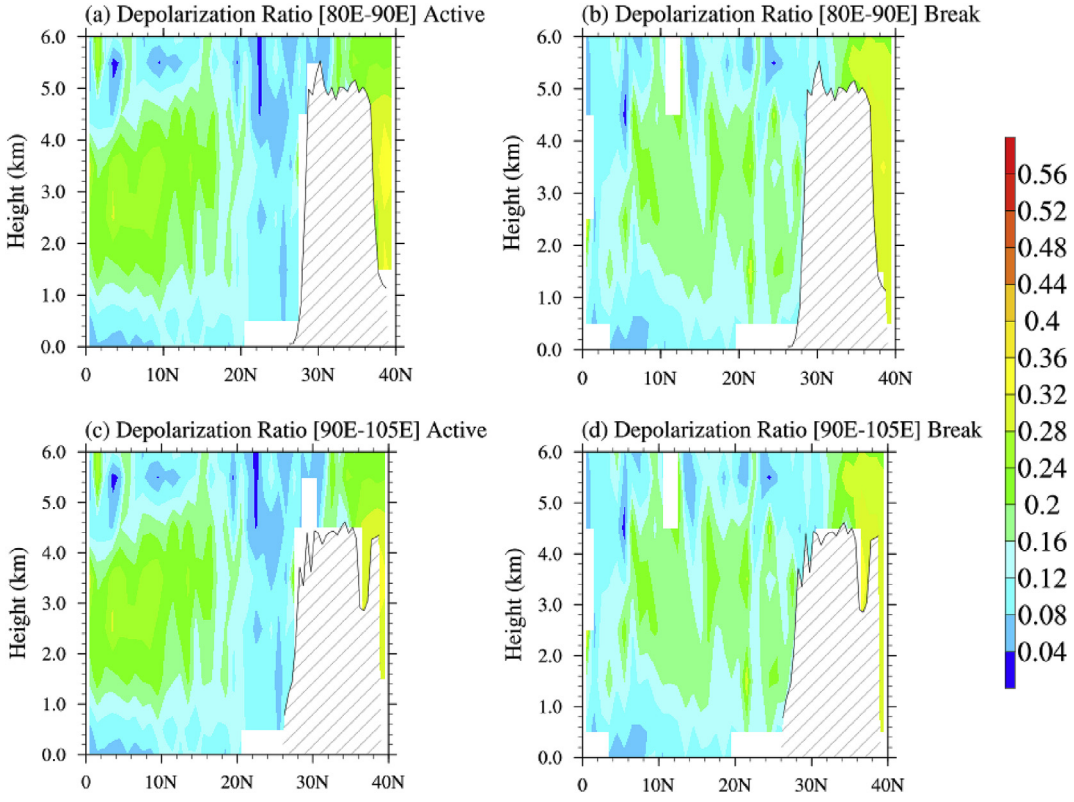

Fig. 5. Latitude-height cross sections of particulate depolarization ratio at 532 nm averaged between 80° E – 90° E and 90° E – 105° E associated with active and break spells during the ASM period. The shaded parts in each plot indicate the topography of the Tibetan Plateau.

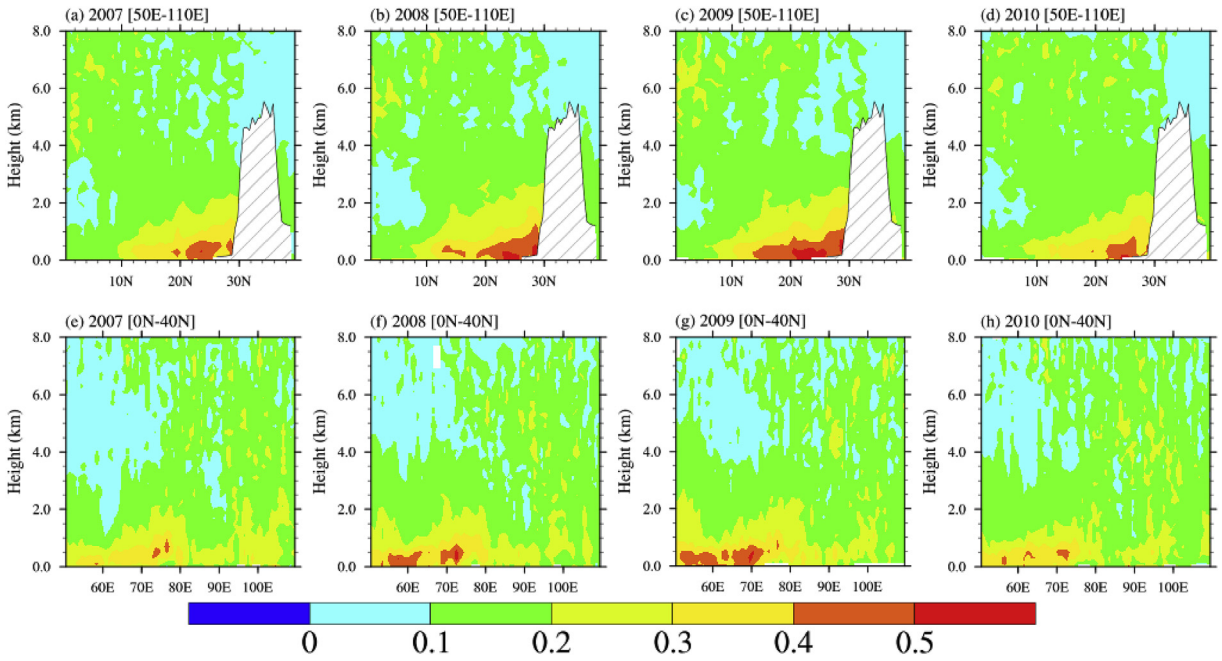

Fig. 6. Latitude-height cross section between 50° and 110° E (upper panel) and longitude-height cross section between 0° and 40° N (lower panel) of aerosol extinction coefficient at 532 nm (unit: km^{-1}) for July and August in 2007, 2008, 2009, 2010. The shaded parts in plots (a)–(d) indicate the topography of the Tibetan Plateau.

section (Fig. 6e, f, g, h) of the mean aerosol extinction coefficient for July and August 2007–2010, which clearly demonstrate the evolution of aerosol extinction coefficient over the four years. Aerosol extinction coefficient associated with ASM in the lower troposphere (3 km) was significantly high over north Arabian Sea, India, Bangladesh, and north Bay of Bengal, which vertically extends up to tropopause between 2007 and 2010 (Fig. 6). The second most extensive aerosol signal demonstrated by aerosol extinction coefficient from the latitude-height cross section was that tropospheric aerosols were transported upward to 8 km from the equatorial Indian Ocean to South Asia (Fig. 6a, b, c, d). Based on the mean variation of tropospheric aerosols over the four years in ASM region, it seems that during the monsoon seasons of 2008 and 2009, tropospheric aerosols were enhanced than those detected in 2007 and 2010 (Figs. 6 and 7). The longitude-height cross section between 0° and 40° N indicated that from west to east of the region, aerosols in the lower troposphere have strong signals, which vertically extended up to the tropopause. This spatial trend agrees well with the results exhibited in Figs. 2, 3 and 7. Furthermore, latitude-height cross sections between 10° and 30° N (averaged at 50°–80° E) and longitude-height cross sections between 50° and 80° E (averaged at 10°–30° N) of aerosol extinction coefficient at 532 nm for July and August in 2007, 2008, 2009, 2010 are shown in Figs. S4 and S5, respectively. The results indicated that tropospheric aerosols were extensive in several vertical layers with the heights of 2 km, 4 km, and 5–7 km. The vertical structure of aerosol in the lower troposphere was more distinct particularly in the longitude-height cross sections (Fig. S5). It is apparent that from the equatorial Indian Ocean to north Arabian Sea and southwest Asia, tropospheric aerosols were vertically distributed and propagated over this sub-region in three layers. It is an interesting finding since over the investigated time series, this has always been the case (Figs. S4 and S5). The high aerosol extinction coefficients over the lower troposphere of India, north Bay of Bengal, and other adjoining areas suggest that atmospheric aerosols transport in the boundary layer was significant. Tropospheric aerosols were transported from west to east of South Asia as revealed from the longitude-height cross section in Figs. 2 and 6. In addition, those tropospheric aerosols can easily cross the TP by long-range transboundary transport from South Asia and other source regions (e.g., Lüthi et al., 2015; Cong et al., 2015), because the ASM circulations offer an effective pathway for water vapor and other atmospheric emissions from the lower troposphere into the upper troposphere (e.g., Park et al., 2004, 2007; Fu et al., 2006). Moreover, the monsoon circulation provides a vertical pathway for atmospheric pollution from South Asia (e.g., India, Bangladesh) to the incursion of the global stratosphere (Randel et al., 2010). Previous study recognized that convective transportation of lower tropospheric materials can affect atmospheric constituents near the tropopause region (Tobo et al., 2007). Particularly the effects of hydration and adiabatic cooling relevant to deep convection over the TP observed using balloon-borne may also trigger enhancement of pre-existing or vertically-transported aqueous solution droplets (e.g., liquid sulfate particles) near the tropopause region (Kim et al., 2003; Tobo et al., 2007). The deposition of light-absorbing aerosols in ATAL on snow and glaciers of the TP has significant impacts on snow darkening, snow and glacier melt, as well as meltwater runoff (e.g., Qian et al., 2011, 2015; Lau et al., 2018). Study on snow and ice samples from glaciers revealed that the presence of carbonaceous particulate matter, with biomass burning identified as account for more than 90% of carbonaceous particles (Pavese et al., 2014). Therefore, enhancement of the tropospheric aerosols should be considered in evaluating the regional or global climate system and the geochemical cycle.

The evolution of the spatial distribution of aerosol particulate depolarization ratio during the monsoon season of 2007–2010 has been investigated by using latitude-height cross section (between 50° E – 110° E) and longitude-height cross section (between 0° N and 40° N) (Fig. 7). The monsoon aerosols signal was more and more extensive from 2007 to 2009, substantial fraction of aerosols layer between 2 and 5 km can be seen from the latitude-height cross section (Fig. 7a, b, c). However, this aerosol layer is not detected in the year of 2010 since it was transported to higher tropopause (Fig. 7d). The vertical extent of aerosols extends even up

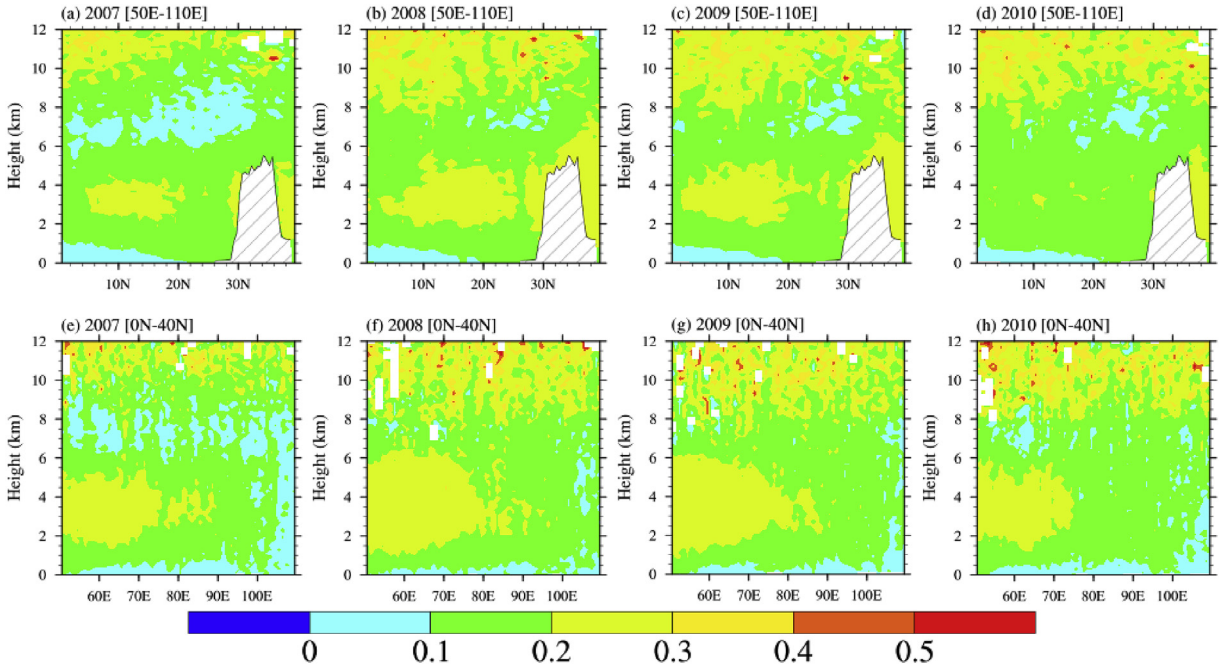

Fig. 7. Latitude-height cross section between 50° E – 110° E (upper panel) and longitude-height cross section between 0° N and 40° N (lower panel) of the mean particulate depolarization ratio at 532 nm for July and August in 2007, 2008, 2009, 2010. The shaded parts in plots (a)–(d) indicate the topography of the Tibetan Plateau.

to 12 km over South Asia and the TP during the monsoon period of 2008, 2009, and 2010. The ATAL aerosols in 2009 and 2010 have the most pronounced signal among the examined four years, this might be due to the volcanic eruption, for example, a large plume of 1.2 Tg of SO_2 and ash was injected above the tropopause after the eruption of Sarychev volcano (Kamchatka, Russia) in June 2009 (Haywood et al., 2010). A large scale volcanic plume had circumnavigated the northern hemisphere for 6 months that was consequently observed in Jul–Aug 2009 by CALIPSO with a SR greater than 1.2 (Vernier et al., 2015); Alaska's Mount Redoubt volcano erupted in March 2009 continued for several months, which represented the most seismic activity occurring on the mountain (Werner et al., 2013). The spatial distribution of aerosols displayed by the longitude-height cross section has similar trend with that revealed from latitude-height cross section. The most obvious aerosols layer was vertically distributed between 2 and 6 km in the atmosphere over the west and southwest Asia. In addition, another detected aerosols layer was widely suspended in the atmosphere at the height of 8–12 km over South Asia, this result is agree well with the trend of aerosols revealed by aerosol extinction coefficient in Fig. 6.

Based on the spatial and temporal distribution of aerosols associated with ASM detected by investigating optical properties of aerosols over South Asia and the TP region, we further examined the characteristics of tropospheric aerosols using SR. Fig. 8 shows the evolution of aerosols associated with ASM over time from 2007 to 2010. The latitude-height cross section (50° E – 110° E) of SR revealed that besides the lower aerosol layer (below 4 km in the atmosphere), there has another aerosol layer primarily at the height of 4–8 km, which is closely consistent with the results detected by using aerosol extinction coefficient, backscatter coefficient, as well as depolarization ratio. The aerosols over the study region were transported northward from equatorial Indian Ocean, cross South Asia, and finally transported to the TP. During the monsoon period of the investigated four years from 2007 to 2010, aerosols were distributed more and more extensively, especially after the 2008, a small fraction of aerosols vertically extended up to 10 km in the troposphere primarily due to deep convection over South Asia. It is worth noting that tropospheric aerosols were simultaneously transported upward and northward from equatorial India Ocean to South Asia. However, tropopause aerosols associated with ASM were most pronounced in South Asia region, reflected from SR latitude-height cross section in Fig. 8, most importantly and interestingly, from equatorial India Ocean to South Asia an upward tilting and ascending structure of aerosols layer can be found during the monsoon season, which typically indicates enhanced aerosol and its optical properties over these regions.

The evolution of SR longitude-height cross section (between 0° N and 40° N) from 2007 to 2010 has been demonstrated in Fig. 9. The spatial distribution of aerosol SR during the monsoon period of the four years is largely consistent. There has been a typical tilting structure of enhanced aerosols over northeast India, north Bay of Bengal, which has been identified in the previous section. It is important to note that from west to east (50° E – 110° E), aerosols signal retrieved by the SR was more intense and distinct, which largely associated with deep convection and emission intensity of source areas. In addition, the low-height aerosols peak is due to locally generated aerosols, while the high-height maximum is most likely due to convectively lifted aerosols that originated at distant sources and subsequently were transported by horizontal upper air movement. In sum, the spatial and temporal distribution pattern of aerosols associated with ASM over South Asia is basically consistent with each other, either from the latitude-height cross section or from longitude-height cross section of SR. Overall, there was a dramatically enhanced aerosols layer, which with tilting structure in the troposphere over the four years, probably it is a natural phenomenon of human-derived aerosols in the troposphere over this region.

3.4. Possible formation mechanisms of the ATAL

The nature and the origin of tropospheric aerosol is a fundamental question for understanding its radiative and chemical

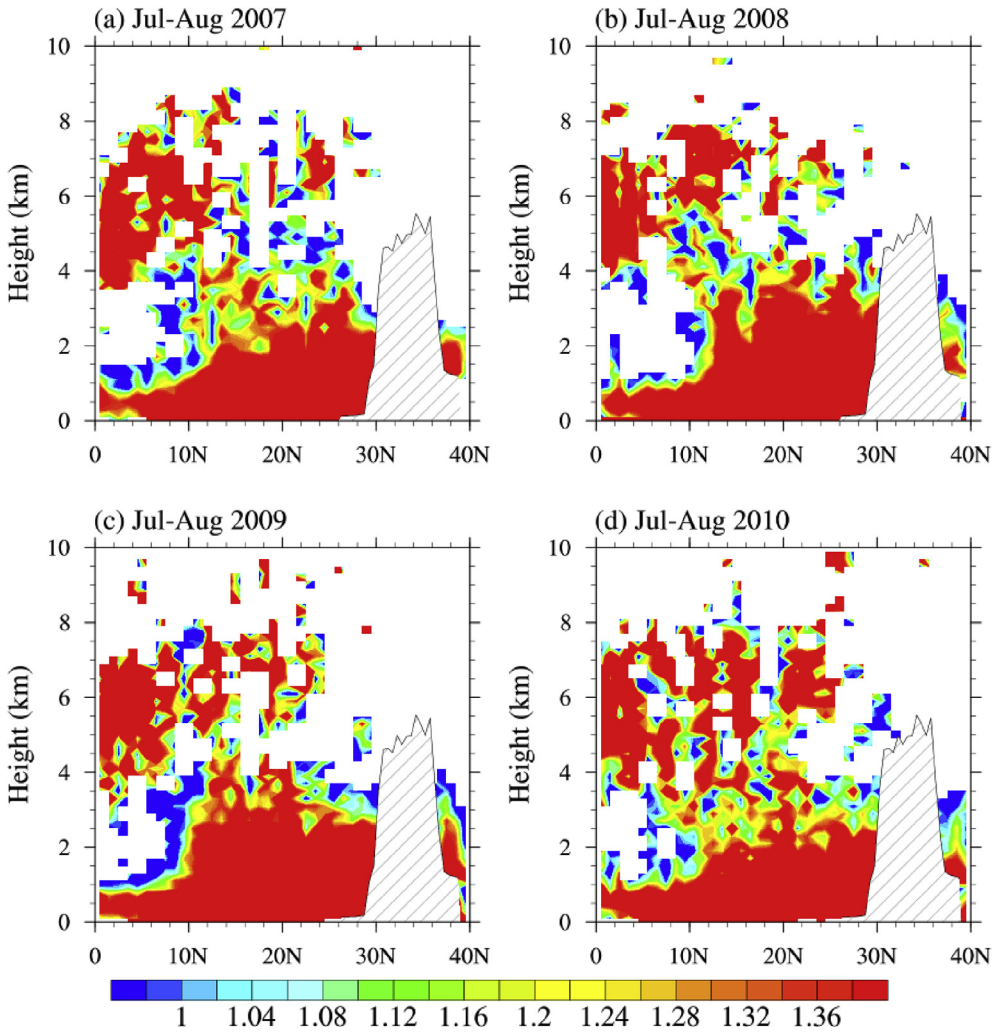

Fig. 8. Mean scattering ratio (SR) latitude-height cross section between 50° E – 110° E for July and August in (a) 2007, (b) 2008, (c) 2009, (d) 2010. The shaded parts in plots (a) and (b) indicate the topography of the Tibetan Plateau.

impact on climate. It was investigated that aerosols at lower heights of the ATAL are largely composed of carbonaceous, sulfate, and organic materials associated with long-range transport of Asian pollutants (Randel et al., 2010) under deep convection over the Indian subcontinent, plus amplification by local input in a large-scale subsidence backdrop (Ravi Kiran et al., 2009; Manoj et al., 2011). Secondary aerosol formation and growth in a cold, moist, and deep convective environment (the monsoon anticyclone is characterized by cold temperate in the upper troposphere) play an important role in the formation of ATAL (Randel and Park, 2006). Secondary organic aerosol, which relevant to extensive biogenic emission from the earth surface, is the dominant component of aerosol mass in the free troposphere, with large implications for inter-continental pollution transport and radiative forcing of climate (Heald et al., 2005; Yu et al., 2015). Moreover, the oxidation of sulfur-containing gaseous pollutants in the tropopause by radical OH (i.e. $OH\cdot$) could lead to generate new micro-particles (Vernier et al., 2009, 2015). Modeling by Neely et al. (2014) suggested that ATAL was mainly the product of human-derived sulfur emissions with at least 30% of the sulfur coming from South Asia. Simulation studies conducted by other groups suggest that South Asian sulfur contributed high percentage to ATAL (Yu et al., 2015) and thus supports the ATAL phenomenon as a recent development. The upward transport of primary aerosols (dust, soot, salt) by deep convection system could result in the formation of an aerosol layer at higher heights, which to a large extent, depending on their solubility with water. The Southeast Asian monsoon also offers a possible vertical pathway for the transport of aerosols from the boundary layer to the upper troposphere (Randel and Park, 2006; Vernier et al., 2011) because the strongest convection occurs over the Indian Ocean and Southeast Asia, on the southeastern edge of the anticyclone (Park et al., 2007). Once transported, aerosol is trapped in the boundary due to large scale deposition relevant to the heat trough in the tropical region (Ravi Kiran et al., 2009).

Moreover, tropopause aerosol enhancement greatly associated with water vapor transportation from the lower troposphere to tropopause which was caused by dynamical upward movement of air mass over the TP during the ASM season (e.g., Kim et al., 2003). The formation of aerosols layers near the tropopause probably impacted by monsoon activities in summer over the TP. Recent study indicated that monsoonal convection over the Indian subcontinent combined with high levels of air pollution from the near surface is mainly responsible for ATAL's formation and impact the global upper tropospheric aerosol budget (Vernier et al., 2015). Aircraft in situ measurements suggest that aerosols at lower heights of the ATAL are largely composed of carbonaceous and

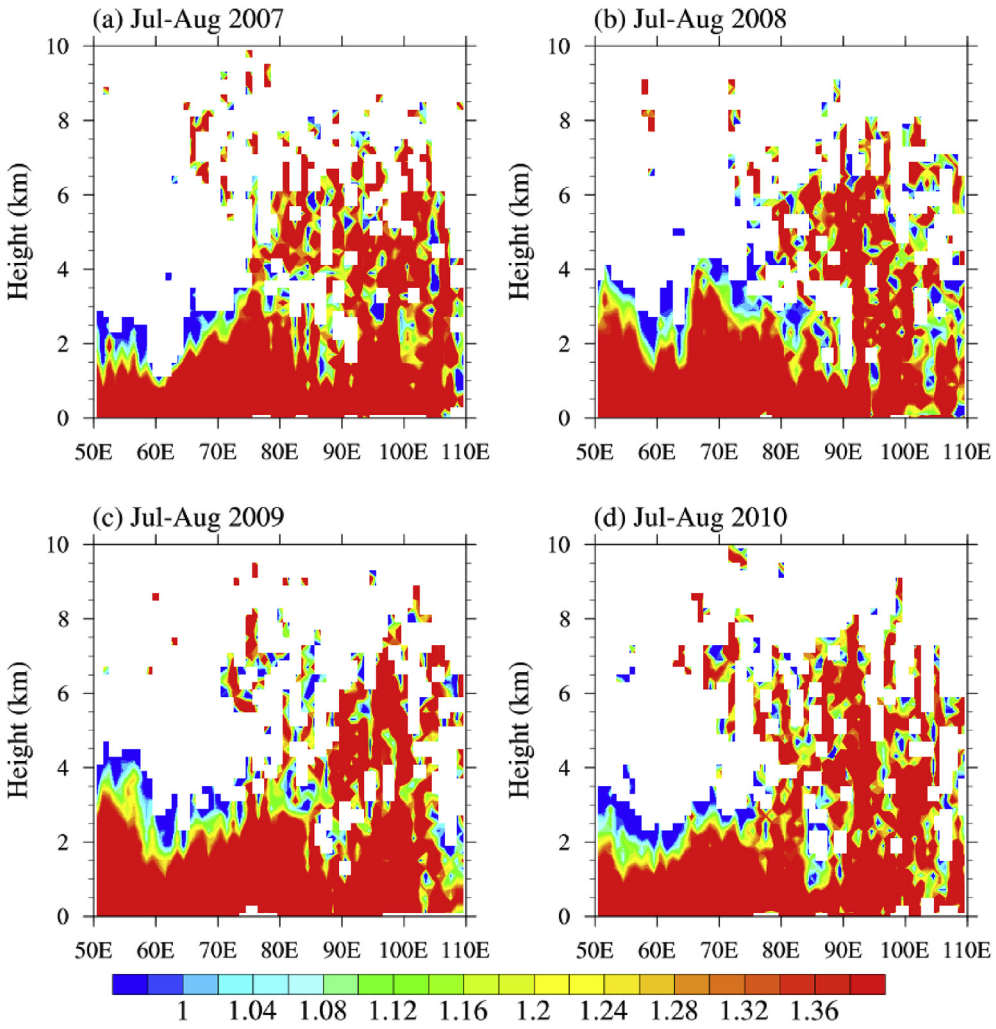

Fig. 9. Mean scattering ratio (SR) longitude-height cross section between 0° N and 40° N for July and August in (a) 2007, (b) 2008, (c) 2009, (d) 2010.

sulfate materials. Carbonaceous particles and their organic components are one of the major combustion by-products, they are identified to play an important role in radiative transfer, air quality, and even human health, due to their fine-micrometric property. Carbonaceous particles also contribute to the extinction of visible light by both scattering and absorption, thus influencing visibility degradation and radiative transfer through the atmosphere (Penner and Novakov, 1996). These effects are magnified by trans-boundary air masses transport of natural fires plumes or anthropogenic emissions from domestic heating, cooking, and industrial activities (Pavese et al., 2014). The tropospheric aerosols are emitted from a mixture of anthropogenic and natural sources. Aerosol climate effects depend on the chemical and physical properties of individual particles (Pósfai and Buseck, 2010). Radiative forcing of the aerosols can intensify the accumulation of aerosol pollution (Ding et al., 2016; Petäjä et al., 2016; Peng et al., 2016). Light-absorbing aerosols can hinder the amount of outgoing spectrum and amplify the greenhouse effect (e.g., Bond et al., 2013; Koch and Del Genio, 2010). Aerosol microparticulates affect the Earth's climate and radiation budget and modify the greenhouse effect (Boucher et al., 2013). The magnitude of this modulation depends on their chemical composition and size distribution determining their close interactions with clouds and radiation (Formenti et al., 2018). These theories are somewhat suitable to be used to decipher the spatial trend of enhanced aerosol backscatter coefficient, extinction coefficient over South Asia regions revealed in this study. The observations and preliminary analyses in this study are, however, still tentative and need to be further refined. More robust investigations are needed to better understand tropospheric aerosols near the TP over the ASM region. It is also necessary to have direct particulate and gaseous speciation measurements near the tropopause to obtain a better understanding of chemical disturbance relating to the tropopause aerosol enhancement.

4. Conclusions

A procedure for studying the evolution of the aerosols in the troposphere using four-year (2007–2010) CALIOP lidar data has been explored. Measurements of aerosol optical and microphysical parameters were used to explore the properties, vertical distribution, and the evolution of tropopause aerosols. A large amount of aerosols, i.e., ATAL, extended up to the tropopause during the monsoon season in the tropic areas. The presence of ATAL during the monsoon season highlights the role of deep convection associated with the ASM in transporting aerosols to the upper troposphere and lower stratosphere. Over the ASM region, enhanced aerosols with a large vertical extent due to deep convection are observed over the north Bay of Bengal, the north Arabian Sea, the

west coast of India, and equatorial Indian Ocean. Convective transport is an important factor controlling the vertical structure of tropopause aerosols during the monsoon season in these regions.

An interesting feature associated with the active convection period revealed in this study is the vertical tilting structure of depolarization ratio over the west and east regions of South Asia. Moreover, the evolution of aerosol SR indicated that from equatorial Indian Ocean to South Asia, there is an upward tilting and ascending structure of the aerosols layer during the monsoon season, which typically indicates enhanced aerosol presence over those emission regions. It is probably a natural phenomenon of human-derived aerosols in the troposphere over this region.

The lower part of the ATAL is largely composed of carbonaceous, sulfate, and organic materials associated with long-range transport of Asian pollutants by deep convection over the Indian subcontinent. Secondary organic aerosol is a major component of aerosol mass in the free troposphere, with potential implications for intercontinental pollution transport and radiative forcing of climate. Information on aerosol size distribution and composition are needed for better understanding the nature and origin of ATAL. Enhancement of the tropospheric aerosols should be considered in future studies in analyzing the regional or global climate system and the geochemical cycles.

5. Main finding of this paper

There exists an upward tilting and ascending structure of the aerosols layer during the monsoon season over the north Arabian Sea, India, north Bay of Bengal, and equatorial Indian Ocean, and finally reached to the southeast of Tibetan Plateau, which typically indicates enhanced aerosols over the Asian monsoon region.

Conflicts of interest

The authors declared that they have no conflicts of interest to this work.

Acknowledgements

This work was supported by the National Natural Science Foundation of China (41601071, 41721091, 41630754), the Independent Program of SKLCS (SKLCS-ZZ-2019) and the National Social Science Foundation of China (17CGJ019). Y. Wang was supported by the U.S. National Science Foundation Atmospheric Chemistry Program. We also thank the support of the Key Research Program for Frontier Sciences of Chinese Academy of Sciences (QYZDJ-SSW-DQC039). The data used in this study were obtained from the NASA Langley Research Center Atmospheric Science Data Center and CALIPSO satellite observations.

Appendix A. Supplementary data

Supplementary data to this article can be found online at https://doi.org/10.1016/j.envpol.2019.06.111.

References

Anderson, T.L., Charlson, R.J., Winker, D.M., John, A.O., Kim, H., 2003. Mesoscale variations of tropospheric aerosols. J. Atmos. Sci. 60, 119–136.

Bond, T.C., Doherty, S.J., Fahey, D.W., Forster, P.M., Berntsen, T., DeAngelo, B.J., Flanner, M.G., Ghan, S., Kärcher, B., Koch, D., Kinne, S., Kondo, Y., Quinn, P.K., Sarofim, M.C., Schultz, M.G., Schulz, M., Venkataraman, C., Zhang, H., Zhang, S., Bellouin, N., Guttikunda, S.K., Hopke, P.K., Jacobson, M.Z., Kaiser, J.W., Klimont, Z., Lohmann, U., Schwarz, J.P., Shindell, D., Storelvmo, T., Warren, S.G., Zender, C.S., 2013. Bounding the role of black carbon in the climate system: a scientific assessment. J. Geophys. Res.-Atmos. 118, 5380–5552. https://doi.org/10.1002/jgrd.50171.

Boucher, O., Randall, D., Artaxo, P., Bretherton, C., Feingold, G., Forster, P., Kerminen, V.M., Kondo, Y., Liao, H., Lohmann, U., Rasch, P., Satheesh, S.K., Sherwood, S., Stevens, B., Zhang, X.Y., 2013. Clouds and aerosols. In: Stocker, T.F., Qin, D., Plattner, G.-K., Tignor, M., Allen, S.K., Boschung, J., Nauels, A., Xia, Y., Bex, V., Midgley, P.M. (Eds.), Climate Change, the Physical Science Basis. Contribution of Working Group I to the Fifth Assessment Report of the Intergovernmental Panel on Climate Change. Cambridge University Press, Cambridge, United Kingdom and New York, NY, USA, pp. 571–658. https://doi.org/10.1017/CBO9781107415324.016.

Cohen, J.B., Prinn, R.G., 2011. Development of a fast, urban chemistry metamodel for inclusion in global models. Atmos. Chem. Phys. 11, 7629–7656.

Cohen, J.B., Loong Ng, D.H., Lim, A.W.L., Chua, X.R., 2018. Vertical distribution of aerosols over the maritime continent during El Niño. Atmos. Chem. Phys. 18, 7095–7108. https://doi.org/10.5194/acp-18-7095-2018.

Cong, Z.Y., Kang, S.C., Kawamura, K., Liu, B., Wan, X., Wang, Z., Gao, S.P., Fu, P., 2015. Carbonaceous aerosols on the south edge of the Tibetan Plateau: concentrations, seasonality and sources. Atmos. Chem. Phys. 15, 1573–1584. https://doi.org/10.5194/acp-15-1573-2015.

Ding, A., Huang, X., Nie, W., Sun, J., Kerminen, V.M., Petäjä, T., Su, H., Cheng, Y., Yang, X., Wang, M., Chi, X., Wang, J., Virkkula, A., Guo, W., Yuan, J., Wang, S., Zhang, R., Wu, Y., Song, Y., Zhu, T., Zilitinkevich, S., Kulmala, M., Fu, C., 2016. Enhanced haze pollution by black carbon in megacities in China. Geophys. Res. Lett. 43, 287–2879. https://doi.org/10.1002/2016GL067745.

Formenti, P., Piketh, S.J., Namwoonde, A., Klopper, D., Burger, R., Cazaunau, M., Feron, A., Gaimoz, C., Broccardo, S., Walton, N., Desboeufs, K., Siour, G., Hanghome, M., Mafwila, S., Omoregie, E., Junkermann, W., Maenhaut, W., 2018. Three years of measurements of light-absorbing aerosols over coastal Namibia: seasonality, origin, and transport. Atmos. Chem. Phys. 18, 17003–17016. https://doi.org/10.5194/acp-18-17003-2018.

Fu, R., Hu, Y., Wright, J.S., Jiang, J.H., Dickinson, R.E., Chen, M., Filipiak, M., Read, W.G., Waters, J.W., Wu, D.L., 2006. Short circuit of water vapor and polluted air to the global stratosphere by convective transport over the Tibetan Plateau. Proc. Natl. Acad. Sci. U.S.A. 103, 5664–5669. https://doi.org/10.1073/pnas.0601584103.

Fu, Q., Hu, Y., Yang, Q., 2007. Identifying the top of the tropical tropopause layer from vertical mass flux analysis and CALIPSO lidar cloud observations. Geophys. Res. Lett. 34, L14813. https://doi.org/10.1029/2007GL030099.

Gettelman, A., Kinnison, D.E., Dunkerton, T.J., Brasseur, G.P., 2004. Impact of monsoon circulations on the upper troposphere and lower stratosphere. J. Geophys. Res. Atmos. 10, 10292004JD004878.

Guo, J., Miao, Y., Zhang, Y., Liu, H., Li, Z., Zhang, W., He, J., Lou, M., Yan, Y., Bian, L., Zhai, P., 2016. The climatology of planetary boundary layer height in China derived from radiosonde and reanalysis data. Atmos. Chem. Phys. 16, 13309–13319. https://doi.org/10.5194/acp-16-13309-2016.

Guo, J., Su, T., Li, Z., Miao, Y., Li, J., Liu, H., Xu, H., Cribb, M., Zhai, P., 2017. Declining frequency of summertime local-scale precipitation over eastern China from 1970 to 2010 and its potential link to aerosols. Geophys. Res. Lett. 44, 5700–5708 doi.10.100 2/2017GL0 73533.

Haarig, M., Ansmann, A., Baars, H., Jimenez, C., Veselovskii, I., Engelmann, R., Althausen, D., 2018. Depolarization and lidar ratios at 355, 532, and 1064 nm and microphysical properties of aged tropospheric and stratospheric Canadian wildfire smoke. Atmos. Chem. Phys. 18, 11847–11861. https://doi.org/10.5194/acp-18-11847-2018.

Haywood, J.M., Jones, A., Clarisse, L., Bourassa, A., Barnes, J., Nicolas, P., 2010. Observations of the eruption of the Sarychev volcano and simulations using the HadGEM2 climate model. J. Geophys. Res. 115, D21212. https://doi.org/10.1029/2010JD014447.

Heald, C.L., Jacob, D.J., Park, R.J., Russell, L.M., Huebert, B.J., Seinfeld, J.H., Liao, H., Weber, R.J., 2005. A large organic aerosol source in the free troposphere missing from current models. Geophys. Res. Lett. 32, L18809. https://doi.org/10.1029/2005GL023831.

Hill, S.C., Smoot, L.D., 2000. Modeling of nitrogen oxides formation and destruction in combustion systems. Prog. Energy Combust. Sci. 26 (4–6), 417–458.

Hodzic, A., Madronich, S., Bohn, B., Massie, S., Menut, L., Wiedinmyer, C., 2007. Wildfire particulate matter in Europe during summer 2003: mesoscale modeling of smoke emissions, transport and radiative effects. Atmos. Chem. Phys. 7, 4043–4064. https://doi.org/10.5194/acp-7-4043-2007.

Holton, J.R., Haynes, P.H., McIntyre, M.E., Douglass, A.R., Rood, R.B., Pfister, L., 1995. Stratosphere-troposphere exchange. Rev. Geophys. 33, 403–440. https://doi.org/10.1029/95RG02097.

Howarth, R.W., 1998. An assessment of human influences on fluxes of nitrogen from the terrestrial landscape to the estuaries and continental shelves of the North Atlantic Ocean. Nutrient Cycl. Agroecosyst. 52 (2–3), 213–223. https://doi.org/10.1023/A:1009784210657.

Huang, J.P., Minnis, B., Chen, Z., Huang, Z., Liu, Q., Zhao, Y.Y., Ayers, J.K., 2008. Long-range transport and vertical structure of Asian dust from CALIPSO and surface measurements during PACDEX. J. Geophys. Res. 113, D23212. https://doi.org/10.1029/2008JD010620.

Jiang, X., Waliser, D.E., Li, J., Woods, C., 2011. Vertical cloud structures of the boreal summer intra-seasonal variability based on CloudSat observations and ERA-interim reanalysis. Clim. Dyn. 36, 2219–2232. https://doi.org/10.1007/s00382-010-0853-8.

Jin, Q.J., Yang, Z.L., Wei, J.F., 2016. Seasonal responses of Indian summer monsoon to dust aerosols in the Middle East, India, and China. J. Clim. 29, 6329–6349. https://doi.org/10.1175/JCLI-D-15-0622.1.

Kim, D., Wang, C., Ekman, A.M.L., Barth, M.C., Rasch, P., 2008. Distribution and direct radiative forcing of carbonaceous and sulfate aerosols in an interactive size-resolving aerosol-climate model. J. Geophys. Res. 113, D16309. https://doi.org/10.1029/2007JD009756.

Kim, Y.S., Shibata, T., Iwasaka, Y., Shi, G.Y., Zhou, X.J., Tamura, K., Ohashi, T., 2003. Enhancement of aerosols near the cold tropopause in summer over Tibetan Plateau: lidar and balloon-borne measurements in 1999 at Lhasa, Tibet, China, Proc. SPIE 4893. In: Lidar Remote Sensing for Industry and Environment Monitoring III. https://doi.org/10.1117/12.466090.

Kipling, Z., Stier, P., Johnson, C.E., Mann, G.W., Bellouin, N., Bauer, S.E., Bergman, T., Chin, M., Diehl, T., Ghan, S.J., Iversen, T., Kirkevåg, A., Kokkola, H., Liu, X., Luo, G., van Noije, T., Pringle, K.J., von Salzen, K., Schulz, M., Seland, Ø., Skeie, R.B., Takemura, T., Tsigaridis, K., Zhang, K., 2016. What controls the vertical distribution of aerosol? Relationships between process sensitivity in HadGEM3-UKCA and inter-model variation from Aero Com Phase II. Atmos. Chem. Phys. 16, 2221–2241. https://doi.org/10.5194/acp-16-2221-2016.

Koch, D., Del Genio, A.D., 2010. Black carbon semi-direct effect on cloud cover: review and synthesis. Atmos. Chem. Phys. 10, 7685–7696. https://doi.org/10.5194/acp-10-7685-2010.

Konovalov, I.B., Beekmann, M., Kuznetsova, I.N., Yurova, A., Zvyagintsev, A.M., 2011. Atmospheric impacts of the 2010 Russian wildfires: integrating modelling and measurements of an extreme air pollution episode in the Moscow region. Atmos. Chem. Phys. 11, 10031–10056. https://doi.org/10.5194/acp-11-10031-2011.

Kremser, S., et al., 2016. Stratospheric aerosol-Observations, processes, and impact on climate. Rev. Geophys. 54, 278–335 doi.10. 1002/2015R G000511.

Lawrence, M.G., et al., 2003. Global chemical weather forecasts for field campaign planning: predictions and observations of large - scale features during MINOS, CONTRACE, and INDOEX. Atmos. Chem. Phys. 3, 267–289. https://doi.org/10.5194/acp-3-267-2003.

Lawrence, M.G., Lelieveld, J., 2010. Atmospheric pollutant outflow from southern Asia: a review. Atmos. Chem. Phys. 10 (11) https://doi.org/10.5194/acp-10-11017-2010, 01 7-11, 096.

Lau, W.K.M., Sang, J., Kim, M.K., Kim, K.M., Koster, R.D., Yasunari, T.J., 2018. Impacts of snow darkening by deposition of light-absorbing aerosols on hydroclimate of Eurasia during boreal spring and summer. J. Geophys. Res. 123, 8441–8461. https://doi.org/10.1029/2018JD028557.

Lau, K.M., Zhou, Y.P., Wu, H.T., 2008. Have tropical cyclones been feeding more extreme rainfall? J. Geophys. Res. 113, D23113. https://doi.org/10.1029/2008JD009963.

Lau, W.K.M., Kim, K.M., Shi, J.J., Matsui, T., Chin, M., Tan, Q., Peters-Lidard, C., Tao, W.K., 2016. Impacts of aerosol–monsoon interaction on rainfall and circulation over Northern India and the Himalaya Foothills. Clim. Dym. https://doi.org/10.1007/s00382-016- 3430-y.

Li, Q.B., et al., 2005. Convective outflow of South Asian pollution: a global CTM simulation compared with Aura MLS observations. Geophys. Res. Lett. 32 https://doi.org/10.1029/2005GL022 762. L1 4826.

Li, Z.X., Feng, Q., Guo, X.Y., Gao, Y., Pan, Y.H., Wang, T.T., Li, J.G., Guo, R., Jia, B., Song, Y.X., 2015. The evolution and environmental significance of glaciochemistry during the ablation period in the north of Tibetan Plateau, China. Quat. Int. 374, 93–109.

Liu, D., Wang, Z., Liu, Z., Winker, D., Trepte, C., 2008b. A height resolved global view of dust aerosols from the first year CALIPSO lidar measurements. J. Geophys. Res. 11 (3), D16214. https://doi.org/10.1029/2007JD009776.

Liu, Z., Liu, D., Huang, J., Vaughan, M., Uno, I., Sugimoto, N., Kittaka, C., Trepte, C., Wang, Z., Hostetler, C., Winker, D., 2008a. Airborne dust distributions over the Tibetan Plateau and surrounding areas derived from the first year of CALIPSO lidar observations. Atmos. Chem. Phys. 8, 5045–5060.

Liu, Q., Ma, X.J., Yu, Y.R., Qin, Y., Chen, Y.H., Kang, Y.M., Zhang, H., Cheng, T.T., Ling, Y., Tang, Y.J., 2017. Comparison of aerosol characteristics during haze periods over two urban agglomerations in China using CALIPSO observations. Particuology 33, 63–72.

Lüthi, Z.L., Škerlak, B., Kim, S.W., Lauer, A., Mues, A., Rupakheti, M., Kang, S., 2015. Atmospheric brown clouds reach the Tibetan Plateau by crossing the Himalayas. Atmos. Chem. Phys. 15, 6007–6021 doi.org/10.5194/acp-15-6007-2015.

Manoj, M.G., Devara, P.C.S., Safai, P.D., Goswami, B.N., 2011. Absorbing aerosols facilitate transition of Indian monsoon breaks to active spells. Clim. Dyn. 37, 2181–2198. https://doi.org/10.1007/s00382-010-0971-3.

Mari, C., Jacob, D.J., Bechtold, P., 2010. Transport and scavenging of soluble gases in a deep convective cloud. J. Geophys. Res. 105 (22) https://doi.org/10.1029/2000JD900211, 255-22, 267.

Ming, Y., Ramaswamy, V., Persad, G., 2010. Two opposing effects of absorbing aerosols on global-mean precipitation. Geophys. Res. Lett. 37 https://doi.org/10.1029/2010GL042895.

Mitchell, J.M., 1970. A preliminary evaluation of atmospheric pollution as a cause of the global temperature fluctuation of the past century. In: Singer, S.F. (Ed.), Global Effects of Environmental Pollution. Springer, Dordrecht. https://doi.org/10.1007/978-94-010-3290-2_15.

Murayama, T., et al., 2001. Ground-based network observation of Asian dust events of april 1998 in east Asia. J. Geophys. Res. 106 (D 16) https://doi.org/10.1029/2000JD900554, 18, 345-18, 360.

Neely III, R.R., Yu, P., Rosenlof, K.H., Toon, O.B., Daniel, J.S., Solomon, S., Miller, H.L., 2014. The contribution of anthropogenic SO_2 emissions to the Asian tropopause aerosol layer. J. Geophys. Res. Atmos. 119, 1571–1579. https://doi.org/10.1002/2013JD020578.

Niemeier, U., Timmreck, C., 2015. What is the limit of climate engineering by stratospheric injection of SO_2? Atmos. Chem. Phys. 15 (16), 9129–9141. https://doi.org/10.5194/a cp-15-9129- 2015.

Niu, H.W., He, Y.Q., Lu, X.X., Xin, H.J., 2014. Chemical composition of rainwater in the yulong snow mountain region, southwestern China. Atmos. Res. 144 (195–206), 195–206.

Niu, H.W., Kang, S.C., Wang, H.L., Zhang, R.D., 2018. Seasonal variation and light absorption property of carbonaceous aerosol in a typical glacier region of the southeastern Tibetan Plateau. Atmos. Chem. Phys. 18, 6441–6460.

Park, M., Randel, W.J., Kinnison, D.E., Garcia, R.R., Choi, W., 2004. Seasonal variation of methane, water vapor, and nitrogen oxides near the tropopause: satellite observations and model simulations. J. Geophys. Res. 109, D03302. https://doi.org/10.1029/2003JD003706.

Park, M., Randel, W.J., Gettelman, A., Massie, S., Jiang, J., 2007. Transport above the Asian summer monsoon anticyclone inferred from Aura MLS tracers. J. Geophys. Res. 112, D16309. https://doi.org/10.1029/20 06JD008294.

Pavese, G., Alados-Arboledas, L., Cao, J.J., Satheesh, S.K., 2014. Carbonaceous Particles in the Atmosphere: Experimental and Modelling Issues Advances in Meteorology, vol. 529850. Hindawi Publishing Corporation, pp. 1–2. https://doi.org/10.1155/2014/529850.

Pei, W.S., Zhang, M.Y., Lai, Y.M., Yan, Z.R., Li, S.Y., 2019. Evaluation of the ground heat control capacity of a novel air-L-shaped TPCT-ground (ALTG) cooling system in cold regions. Energy 179, 655–668.

Peng, J., Hu, M., Guo, S., Du, Z., Zheng, J., Shang, D., Levy Zamora, M., Zeng, L., Shao, M., Wu, Y.S., Zheng, J., Wang, Y., Glen, C.R., Collins, D.R., Molina, M.J., Zhang, R., 2016. Markedly enhanced absorption and direct radiative forcing of black carbon under polluted urban environments. Proc. Natl. Acad. Sci. U.S.A. 113, 4266–4271. https://doi.org/10.1073/pnas.1602310113.

Penner, J.E., Novakov, T., 1996. Carbonaceous particles in the atmosphere: a historical perspective to the fifth international conference on carbonaceous particles in the atmosphere. J. Geophys. Res. 101 (D14), 19, 373-19, 378.

Petetin, H., Sauvage, B., Parrington, M., Clark, H., Fontaine, A., Athier, G., Blot, R., Boulanger, D., Cousin, J.-M., Nédélec, P., Thouret, V., 2018. The role of biomass burning as derived from the tropospheric CO vertical profiles measured by IAGOS aircraft in 2002-2017. Atmos. Chem. Phys. 18, 17277–17306. https://doi.org/10.5194/acp-18-17277-2018.

Petäjä, T., Järvi, L., Kerminen, V.M., Ding, A.J., Sun, J.N., Nie, W., Kujansuu, J., Virkkula, A., Yang, X., Fu, C.B., Zilitinkevich, S., Kulmala, M., 2016. Enhanced air pollution via aerosol-boundary layer feedback in China. Sci. Rep. 6, 18998. https://doi.org/10.1038/srep18998.

Pósfai, M., Buseck, P.R., 2010. Nature and climate effects of individual tropospheric aerosol particles. Annu. Rev. Earth Planet Sci. 38, 17–43.

Prakash, P.J., Stenchikov, G., Kalenderski, S., Osipov, S., Bangalath, H., 2015. The impact of dust storms on the Arabian Peninsula and the red Sea. Atmos. Chem. Phys. 15, 199–222.

Qian, Y., Flanner, M.G., Leung, L.R., Wang, W., 2011. Sensitivity studies on the impact s of Tibetan Plat eau snow pack pollution on the Asian hydrological cycle and monsoon climate. Atmos. Chem. Phys. 11 (5), 1929–1948. https://doi.org/10.5194/acp-11-1929-2011.

Qian, Y., Yasunari, T.J., Doherty, S.J., Flanner, M.G., Lau, W.K.M., Ming, J., 2015. Light-absorbing particles in snow and ice: measurement and modeling of climatic and hydrological impact. Adv. Atmos. Sci. 32 (1), 64–91. https://doi.org/10.1007/s00376-014-0010-0.

Ramanathan, V., Chung, C., Kim, D., Betge, T., Buja, L., Kiehl, J.T., Washington, W.M., Fu, Q., Sikka, D.R., Wild, M., 2005. Atmospheric brown clouds: impacts on South Asian climate and hydrological cycle. Proc. Natl. Acad. Sci. U.S.A. 102, 5326–5333. https://doi.org/10.1073/pnas.0500656102.

Randel, W.J., Park, M., 2006. Deep convective influence on the Asian summer monsoon anticyclone and associated tracer variability observed with Atmospheric Infrared Sounder (AIRS). J. Geophys. Res. 111, D12314. https://doi.org/10.1029/2005JD006490.

Randel, W.J., Park, M., Emmons, L., Kinnison, D., Bernath, P., Walker, K.A., Boone, C., Pumphrey, H., 2010. Asian monsoon transport of pollution to the stratosphere. Science 328 (5978), 611–613. https://doi.org/10.1126/science.1182274.

Rajeevan, M., Gadgil, S., Bhate, J., 2010. Active and break spells of the Indian summer monsoon. J. Earth Syst. Sci. 3, 229–247.

Rajeevan, M., Rohini, P., Niranjan Kumar, K., Srinivasan, J., Unnikrishnan, C.K., 2013. A study of vertical cloud structure of the Indian summer monsoon using CloudSat data. Clim. Dyn. 40, 637–650. https://doi.org/10.1007/s00382-012-1374-4.

Ravi Kiran, V., Rajeevan, M., Bhaskara Rao, S.V., Prabhakara Rao, N., 2009. Analysis of variations of cloud and aerosol properties associated with active and break spells of Indian summer monsoon using MODIS data. Geophys. Res. Lett. 36, L09706. https://doi.org/10.1029/2008GL037135.

Rosenfeld, D., Fromm, M., Trentmann, J., Luderer, G., Andreae, M.O., Servranckx, R., 2007. The Chisholm firestorm: observed, precipitation and lightning activity of a pyro-cumulonimbus. Atmos. Chem. Phys. 7, 645–659.

Solomon, S., Daniel, J.S., Neely III, R.R., Vernier, J.P., Dutton, E.G., Thomason, L.W., 2011. The persistently variable "background" stratospheric aerosol layer and global climate change. Science 33, 866–870.

Tao, W.K., Chen, J.P., Li, Z.Q., Wang, C., Zhang, C.D., 2012. The Impact of Aerosol on convective cloud and precipitation. Rev. Geophys. 50, RG2001. https://doi.org/10.1029/2011RG000369.

Tobo, Y., Iwasaka, Y., Shi, G.Y., Kim, Y.S., Ohashi, T., Tamura, K., Zhang, D.Z., 2007. Balloon-borne observations of high aerosol concentrations near the

summertime tropopause over the Tibetan Plateau. Atmos. Res. 84, 233–241.
Tian, P.F., Cao, X.J., Zhang, L., Sun, N.X., Sun, L., Timothy, L., Shi, J.S., Wang, Y., Ji, Y.M., 2017. Aerosol vertical distribution and optical properties over China from long-term satellite and ground-based remote sensing. Atmos. Chem. Phys. 17, 2509–2523. https://doi.org/10.5194/acp-17-2509-2017.
Thomason, L.W., Pitts, M.C., Winker, D.M., 2007. CALIPSO observations of stratospheric aerosols: a preliminary assessment. Atmos. Chem. Phys. 7, 5283–5290.
Thomason, L.W., Vernier, J.P., 2013. Improved SAGE II cloud/aerosol categorization and observations of the Asian tropopause aerosol layer: 1989-2005. Atmos. Chem. Phys. 13, 4605–4616. https://doi.org/10.5194/acp-13-4605- 2013.
Vernier, J.P., Pommereauet, J.P., Garnieral, A., Pelon, J., Larsen, N., 2009. Tropical stratospheric aerosol layer from CALIPSO lidar observations. J. Geophys. Res. 114, D00H10. https://doi.org/10.1029/2009JD011946.
Vernier, J.P., Thomason, L.W., Kar, J., 2011. CALIPSO detection of an Asian tropopause aerosol layer. Geophys. Res. Lett. 38, L07804. https://doi.org/10.1029/2010GL046614.
Vernier, J.P., Fairlie, T.D., Natarajan, M., Wienhold, F.G., Bian, J., Martinsson, B.G., Crumeyrolle, S., Thomason, L.W., Bedka, K.M., 2015. Increase in upper tropospheric and lower stratospheric aerosol levels and its potential connection with Asian pollution. J. Geophys. Res. Atmos. 120, 1608–1619 doi.10.100 2/2014JD022372.
Werner, C., Kelly, P.J., Doukas, M., Lopez, T., Pfeffer, M., McGimsey, R., Neal, C., 2013. Degassing of CO_2, SO_2, and H_2S associated with the 2009 eruption of Redoubt volcano, Alaska. J. Volcanol. Geotherm. Res. 259, 270–284.
Winker, D.M., Hunt, W.H., McGill, M.J., 2007. Initial performance assessment of CALIOP. Geophys. Res. Lett. 34, L19803 doi.10.102 9/2007GL030135.
Winker, D.M., Pelon, J., Coakley Jr., J.A., Ackerman, S.A., Charlson, R.J., Colarco, P.R., Flamant, P., 2010. The CALIPSO mission: a global 3D view of aerosols and clouds. Bull. Am. Meteorol. Soc. 91, 1211–1229. https://doi.org/10.1175/2010BAMS3009.1.
Winker, D.M., Tackett, J.L., Getzewich, B.J., Liu, Z., Vaughan, M.A., Rogers, R.R., 2013. The global 3-D distribution of tropospheric aerosols as characterized by CALIOP. Atmos. Chem. Phys. 13, 3345–3361.
Wang, C., 2013. Impact of anthropogenic absorbing aerosols on clouds and precipitation: a review of recent progresses. Atmos. Res. 122, 237–249.
Wang, C., 2004. A modeling study on the climate impacts of black carbon aerosols. J. Geophys. Res. 109, D03106. https://doi.org/10.1029/2003JD004084.
Wang, C., 2007. Impact of direct radiative forcing of black carbon aerosols on tropical convective precipitation. Geo phys. Res. Lett. 34, L05709. https://doi.org/10.1029/2006GL028416.
Wang, C., 2009. The sensitivity of tropical convective precipitation to the direct radiative forcings of black carbon aerosols emitted from major regions. Ann. Geophys. 27, 3705–3711.
Wang, X., Liu, J., Che, H.Z., 2018. Spatial and temporal evolution of natural and anthropogenic dust events over northern China. Sci. Rep. 8, 2141.
Wang, X.P., Yao, T.D., Cong, Z.Y., Yan, Y., Kang, S.C., Zhang, Y.L., 2006. Gradient distribution of persistent organic contaminants along northern slope of central-Himalayas, China. Sci. Total Environ. 372 (1), 193–202.
Yamasoe, M.A., Sauvage, B., Thouret, V., Nédélec, P., Le Flochmoen, E., Barret, B., 2015. Analysis of tropospheric ozone and carbon monoxide profiles over South America based on MOZAIC/IAGOS database and model simulations. Tellus B 67, 27884. https://doi.org/10.3402/tellusb.v67.27884.
Yu, P., Toon, O.B., Neely, R.R., Martinsson, B.G., Brenninkmeijer, C.A.M., 2015. Composition and physical properties of the Asian tropopause aerosol layer and the north American tropospheric aerosol layer. Geophys. Res. Lett. 42, 2540–2546. https://doi.org/10.1002/2015GL063181.
Yu, H., Chin, M., Winker, D.M., Omar, A.H., Liu, Z., Kittaka, C., Diehl, T., 2010. Global view of aerosol vertical distributions from CALIPSO lidar measurements and GOCART simulations: regional and seasonal variations. J. Geophys. Res. 115, D00H30. https://doi.org/10.1029/2009JD013364.
Zhang, R., Wang, Y., He, Q., Chen, L., Zhang, Y., Qu, H., Smeltzer, C., Li, J., Albarado, L., Vrekoussis, M., Richter, A., Wittrock, F., Burrows, J., 2017. Enhanced trans-Himalaya Pollution transport to the Tibetan Plateau by cut-off low systems. Atmos. Chem. Phys. 17, 3083–3095. https://doi.org/10.5194/acp-17-1-2017.